Temperature effects in spin-dependent Hall currents in an ideal skyrmion gas

Andrei Zadorozhnyi and Yuri Dahnovsky

Department of Physics and Astronomy/3905

1000 E. University Avenue

University of Wyoming

Laramie, WY 82071[*]

(Dated: July 16, 2021)

Abstract

The quest of novel reliable and fast performing logic and memory elements in classical and quantum computing requires discoveries of new effects in novel quantum materials. Skyrmions are such magnetic textures where electron scattering can essentially change the shape and location of the skyrmion, which can be used as a memory element being more efficient than domain walls as memory device in classical computing. Because the skyrmion motion is sensitive even to very small currents, we study electron scattering by skyrmions in an ideal skyrmion gas in ferromagnetic environment. In such systems, the direct and Hall currents become spin-dependent. For applications it is important to consider a Hall effect in the whole range of temperatures under the assumption of the skyrmion existence. In this study we find the nonmonotonic temperature dependence of the direct spin-up conductivity, i. e., the conductivity for the current directed along the applied electric field due to the electrons with the spin parallel to the ferromagnetic moment. Such a behavior contradicts the traditional understanding where the temperature only increases the value of the conductivity. The spin-down Hall conductivity is found to be even more dramatic exhibiting the conductivity sign change (i.e., the change in the current direction) with temperature for small skyrmion sizes, $d = 3.7$ nm. Such small skyrmions were observed in a PdFe bilayer on the Ir(111) surface. The found effects strongly depend on Fermi energy. The most pronounced dependencies take place if the Fermi energy is slightly below and above the bottom of the upper (spin-down) energy band of an ideal 2D electron gas. In addition, we also find that the direct and Hall resistivities, ρ_{xx} and ρ_{xy}, are independent of the exchange integral J for $2J > \varepsilon_F$.

I. INTRODUCTION

Magnetic skyrmions are topologically nontrivial spin textures with an additional invariant, topological charge. This property determines an additional stability of the system, and, therefore, can be used for high-density memory, quantum computing, and logic elements for unconventional and neuromorphic computing[1–7]. For high-density memory applications, the skyrmion manipulation can be performed by currents, which are several orders of magnitude smaller, and, therefore, less dissipative, than in the case of traditional domain-wall memory devices.[8–11] Such small current values indicate the importance of spin-dependent Hall conductivities that can take place due to the scattering of conduction electrons by skyrmion textures.[12–15]

Indeed, the needs of high-speed performance electronic devices for various applications require novel materials and new physical phenomena. As shown in Ref.[15], the spin-dependent Hall effect can be efficiently employed for filtering, switching, and separation of spin currents. For some values of the parameters (conduction electron concentrations and skyrmion sizes) it is possible to separate Hall currents for different electron spin projections similar to the charge separation in a charge Hall effect. The spin-filtering, the ability to block spin-down or spin-up currents can be efficiently modulated by changing the electron concentration in a very narrow range.[15]

Electric current can take place because of an applied voltage and also temperature difference between two terminals of a device. In the latter case, the conduction electrons are scattered by an ideal skyrmion gas resulting in spin-dependent Seebeck and Nernst effects.[16–24] As shown in Ref.[25], the spin-dependent Seebeck and Nernst coefficients exhibit substantial nonlinear behaviors with respect to electron concentrations and skyrmion/vortex sizes. Moreover, the abrupt voltage sign change takes place in the narrow range of the electron concentrations.

In the previous research,[25] the spin-dependent Seebeck/Nernst effects were studied in the low temperature limit ($kT \ll \varepsilon_F$). However, the temperature dependence of the direct and Hall conductivities can be important in some materials with certain electron concentrations and energy band structures. In order to study the temperature dependencies, we consider a system of 2D free electrons with the energy band structure depicted in Fig. 1. As shown in this figure, the lower energy band represents spin-up electron energies, while the upper

band represents spin-down ones. The bands are split by a ferromagnetic moment with the exchange integral J.

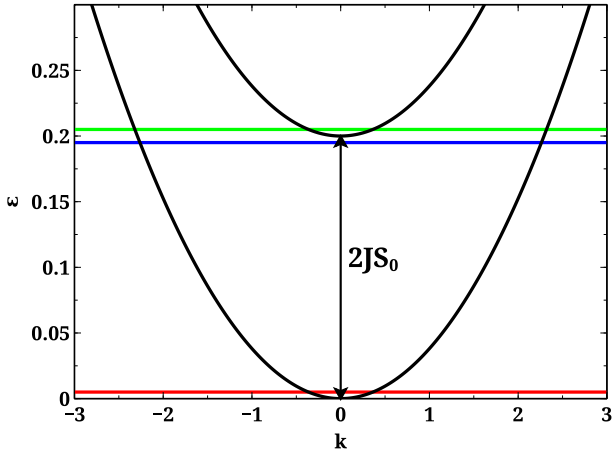

FIG. 1. Energy band structure crossection for 2D conduction electrons. The upper curve stands for electrons with spin-down, and the lower one denotes the energy band for electrons with spin-up. The red line represents ε_F close to the bottom of the lower (spin-up) energy band. The splitting between the bands is $2JS_0$ where J is the exchange integral between the localized and conduction electrons (see Eq. (1)).

In this work we study a spin-dependent Hall effect for electrons scattered by static skyrmions at different temperatures for specific ε_F values as depicted in Fig. 1. The choice of ε_F is determined by the conditions where the temperature effect is pronounced at most. The blue line denotes ε_F slightly lower than the minimum of the upper band. If the temperature is turned on, the electrons with spin-down will populate the upper band and, therefore, this effect will reflect the spin-down electron scattering in an ideal skyrmion gas. We assume that skyrmions are not affected by electric current and temperature. The green line stands for ε_F that is slightly above the minimum of the upper energy surface. In this case, the population of the spin-down electrons increases with the temperature. As demonstrated in this research, the spin-dependent direct and Hall components of electric conductivity are strongly driven by temperature, energy concentrations, and skyrmion sizes. The direct and Hall conductivities are calculated by using the numerical solutions of the Boltzmann equation for a nonequilibrium distribution function and the Lippmann-Schwinger equation for the transition matrix. The scattering mechanism for electrons is determined by

the electron-skyrmion interaction (see Eq. (1)).

II. CALCULATION DETAILS

In order to describe the conduction 2D electron scattering by spin-textures (skyrmions), noninteracting and randomly distributed in space, we consider the electron system described by the following s-d Hamiltonian:

$$H = \frac{\hbar^2 k^2}{2m}\hat{\mathbf{1}} - \mathbf{JS}(\mathbf{r}) \cdot \boldsymbol{\sigma} + \mathbf{JS_0}\hat{\mathbf{1}}, \tag{1}$$

where the first term represents the kinetic energy of conduction electrons, J is an exchange integral, $\mathbf{S}(\mathbf{r})$ is a localized magnetic moment. Here $\boldsymbol{\sigma}$ is a vector with the three Pauli matrix projections for the conduction electron spins. The last term $JS_0\hat{\mathbf{1}}$ is introduced for convenience in order to shift all energy bands upwards by JS_0. We choose the $\mathbf{S}(\mathbf{r})$ texture in the following form:

$$\mathbf{S}(\mathbf{r}) = S_0 \cdot \mathbf{e}_z + \sum_i \delta\mathbf{S}(\mathbf{r} - \mathbf{r_i}), \tag{2}$$

where S_0 is uniform out-of-plane background magnetization and $\delta\mathbf{S}(\mathbf{r} - \mathbf{r_i})$ is a deviation of magnetic moment due to the presence of the magnetic texture (we only consider skyrmions with the topological charge $Q = 1$). In this work we assume a skyrmion shape is not affected by temperature and electric current. The analytical form of the magnetic moment distribution is chosen as follows[12,15,25,26]:

$$\begin{aligned} n_z(r) &= \begin{cases} 4\left(\frac{r}{a}\right)^2 - 2, & r \le a/2, \\ -4\left(1 - \frac{r}{a}\right)^2, & a/2 < r \le a, \\ 0, & r > a, \end{cases} \\ n_x(\boldsymbol{r}) &= \sqrt{1 - (n_z(r)+1)^2}\cos\alpha, \\ n_y(\boldsymbol{r}) &= \sqrt{1 - (n_z(r)+1)^2}\sin\alpha, \end{aligned} \tag{3}$$

where a is the radius of the skyrmion, r is a radius and α is a polar angle in a polar frame with the center of the skyrmion located at $r = 0$. In a more general case we should use $\alpha + \alpha_0$ instead of α to distinguish Bloch and Neel skyrmions where $\alpha_0 = \pm\pi/2$ represents Bloch and $\alpha_0 = 0$ stands for Neel skyrmions. However, as shown in Appendix I, $W^{ss'}_{\boldsymbol{kk'}}$ in

Eq. (6) are independent of α_0. Therefore, the results of the calculations are insensitive to a skyrmion type.

The spin-dependent direct and Hall components are found using the following equations:[24]

$$j^s_{x,y} = e \int v_{x,y} f^s_1(\mathbf{k}) dk_x dk_y, \tag{4}$$

where $v_{x,y}$ is a conduction electron velocity, and $f^s_1(\mathbf{k})$ is the first order correction to the equilibrium distribution function, which can be found from the following stationary integral matrix Boltzmann equation:[24]

$$\frac{\partial f_0}{\partial \varepsilon} e\boldsymbol{E} \cdot \boldsymbol{v}^s = \sum_{s'} \sum_{\boldsymbol{k}'} \left(W^{ss'}_{\boldsymbol{k}\boldsymbol{k}'} f^{s'}_1(\boldsymbol{k}') - W^{s's}_{\boldsymbol{k}'\boldsymbol{k}} f^s_1(\boldsymbol{k}) \right), \tag{5}$$

where $W^{ss'}_{\boldsymbol{k}\boldsymbol{k}'}$ is a transition probability from the state with wavevector $\boldsymbol{k}'$ and spin s' to the state with wavevector $\boldsymbol{k}$ and spin s. f_0 is the equilibrium Fermi distribution function. $\boldsymbol{E} = E\boldsymbol{e}_x$ is an applied electric field. In case of very small skyrmions of in their absence, Boltzmann equation (5) becomes invalid because of the lack of scatters. In this case other scattering mechanisms should be introduced (impurities, electron-phonon, etc.). In this work we consider only the electron-skyrmion scattering mechanism. There is another approach[13,27] where the emergent magnetic and electric fields can be introduced into the dynamic (the left-hand side) part of the Boltzmann equation. The scattering mechanism in this case is not due to the electric scattering by the spin texture. This approach is different from what we use in this research. The emergent field approach requires the introduction of other electron scattering mechanisms, which are not considered in this work. The transition probability can be calculated in terms of transition matrix $T^{ss'}_{\mathbf{k}\mathbf{k}'}$:[28]

$$W^{ss'}_{\boldsymbol{k}\boldsymbol{k}'} = \frac{2\pi}{\hbar} n_{sk} \left| T^{ss'}_{\boldsymbol{k}\boldsymbol{k}'} \right|^2 \delta(\varepsilon - \varepsilon'). \tag{6}$$

Here n_{sk} is a skyrmion density. Electric currents (4) and, therefore, conductivities are inversely proportional to n_{sk}. The transition matrix can be found from the following Lippmann-Schwinger equation:

$$\hat{T} = \hat{V} + \hat{V}\hat{G}_0\hat{T}, \tag{7}$$

where $\hat{G}_0$ is a retarded free electron Green's function determined in the following way:

$$\hat{G}_0(\varepsilon) = \lim_{\delta \to +0} \left[\left(\varepsilon - \frac{\hbar^2 k^2}{2m} \right) \hat{\mathbf{1}} + J\boldsymbol{S}_0 \cdot \hat{\boldsymbol{\sigma}} + i\delta\hat{\mathbf{1}} \right]^{-1}, \tag{8}$$

and V is the potential energy for a single spin texture that is given by the matrix:

$$\hat{V}(\mathbf{r}) = -J \begin{pmatrix} S_z & S_x - iS_y \\ S_x + iS_y & -S_z \end{pmatrix}. \tag{9}$$

To find the solutions of Lippmann-Schwinger (7) and Boltzmann equations (5), we have developed the original codes. The interaction matrix $\hat{V}$ has been considered in a k-space where the wavefunctions have been represented in terms of ordinary plane waves:

$$V_{ss'}(\boldsymbol{k}, \boldsymbol{k}') = \left\langle \boldsymbol{k}s \middle| \hat{V} \middle| \boldsymbol{k}'s' \right\rangle = \frac{1}{(2\pi)^2} \int e^{i(\boldsymbol{k}'-\boldsymbol{k})\cdot\boldsymbol{r}} V_{ss'}(\boldsymbol{r}) \, \mathrm{d}^2\mathrm{r} \tag{10}$$

The retarded Green's function, Eq. (8), has been numerically calculated with the δ value chosen to be much lesser than the Fermi energy. Lippman-Schwinger equation (7) has been solved in a k-space in all orders of $\hat{V}$ using the piecewise-constant approximation of the function $T_{ss'}(\boldsymbol{k}, \boldsymbol{k}') = \left\langle \boldsymbol{k}s \middle| \hat{T} \middle| \boldsymbol{k}'s' \right\rangle$. In order to accelerate the calculations, we have used the H-adaptive mesh methodology. The higher density mesh has been selected in the vicinity of the $\hat{G}_0$ singularities (see Eq. (8)). The lower density mesh has been employed for the grid cells located far away from the singularity curve. The schematic drawing is shown in Fig. 2.

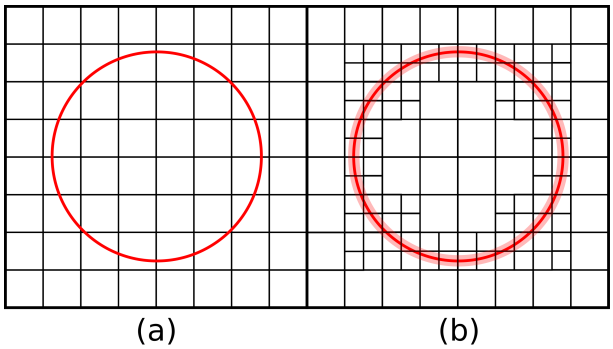

FIG. 2. Schematic sketch of (a) the uniform mesh and (b) the adaptive nonuniform mesh with the thin red circle denoting the $\hat{G}_0$ singularity curve and pale red area around it is its vicinity where we need the function $T_{ss'}(\boldsymbol{k}, \boldsymbol{k}')$ to be calculated with the higher precision. Only one step of the adaptive algorithm is presented.

The structure of the nonequilibrium distribution function is described by the two-element column $(f^{\uparrow}(\boldsymbol{k}), f^{\downarrow}(\boldsymbol{k}))$. As soon as the T-matrix is known and the W-rates are found from

equation (6), the solution of Boltzmann equation (5) has been determined in the piecewise-constant approximation using the same dense mesh in the vicinity of the $\hat{G}_0$ singularity curve. The complexity of the solution is determined by the integral part of the collision integral in the k-space where the integrand contains the very narrow function close to the δ-function in Eq. (6). Such difficulty has been overcome by performing the additional integration of both left and right parts of the equation in the k-space for each mesh cell.

III. RESULTS AND DISCUSSION

It is well-known from statistical mechanics[29] that the equilibrium distribution function for non-interacting fermions is determined from the following expression:

$$f_0(\varepsilon_s, T, \mu(\varepsilon_F, T)) = \frac{1}{\exp\left(\frac{\varepsilon_s - \mu(\varepsilon_F, T)}{k_B T}\right) + 1}, \tag{11}$$

where $\varepsilon_s(\boldsymbol{k})$ is the conduction electron energy that can be determined from Eq. (12):

$$\begin{aligned} \varepsilon_\uparrow &= \frac{\hbar^2 k^2}{2m}, \\ \varepsilon_\downarrow &= \frac{\hbar^2 k^2}{2m} + 2J, \end{aligned} \tag{12}$$

and $\mu(\varepsilon_F, T)$ is chemical potential found from the following expression:[24]

$$\begin{aligned} N &= \frac{1}{(2\pi)^2} \sum_s \int \mathrm{dk_x dk_y} f_0(\varepsilon_s(k_x, k_y), T = 0, \varepsilon_F) \\ &= \frac{1}{(2\pi)^2} \sum_s \int \mathrm{dk_x dk_y} f_0(\varepsilon_s(k_x, k_y), T, \mu(\varepsilon_F, T)), \end{aligned} \tag{13}$$

where N is the electron concentration and $\mu(\varepsilon_F, T = 0) = \varepsilon_F$. The solution of equation (13) is given by the following expression:

$$\mu = k_B T \log\left[\sqrt{\cosh^2 \frac{J}{k_B T} + e^{\frac{\epsilon}{k_B T}} - 1} - \cosh \frac{J}{k_B T}\right], \tag{14}$$

where

$$\epsilon = \begin{cases} 0, \text{ if } \varepsilon_F < 0, \\ \varepsilon_F + J, \text{ if } 0 < \varepsilon_F < 2J, \\ 2\varepsilon_F, \text{ if } \varepsilon_F > 2J. \end{cases} \tag{15}$$

The function $\mu(\varepsilon_F, T)$ is presented in Fig. 3. As shown in Fig. 3a, μ decreased towards negative values for the Fermi energy close to the bottom of the lower band (the red curve).. At high temperatures the Fermi distribution function becomes the Boltzmann distribution function.[24] If ε_F is close to the bottom of the upper energy band (the blue and green curves), the chemical potential is almost insensitive to temperature because of the low temperature limit, $\varepsilon_F \gg k_B T$, under the assumption that

$$2JS_0 \gg k_B T. \tag{16}$$

For estimations, we assume that $JS_0 = 0.1$ eV. In Fig. 3b we see that there are two dips in the ε_F dependencies. One dip is located close to the bottom of the lower energy band, and the other is close to the bottom of the upper band.

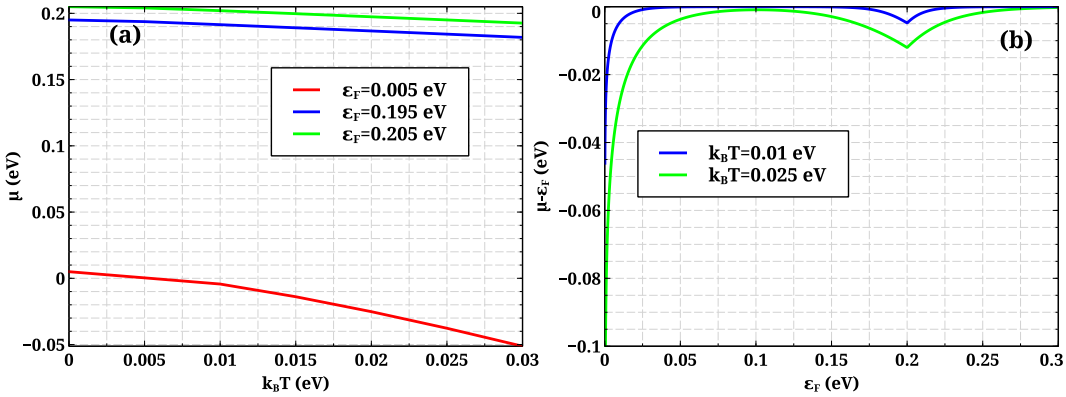

FIG. 3. Dependence of (a) chemical potential, $\mu(\varepsilon_F, T)$, on temperature for three different values of ε_F and (b) $\mu(\varepsilon_F, T) - \varepsilon_F$ on Fermi energy for three different temperatures.

A. Spin-dependent direct current

In Fig. 4 we study the dependence of the direct current (the conductivity) on Fermi energy for both spin-up (Figs. 4a, b, c) and spin-down (Figs. 4d, e, f) components at the three different temperatures $k_B T = 0,\ 0.1J$, and $0.25J$. The skyrmion sizes are $\varkappa a = 3,\ 5$, and 15, where $\varkappa$ is defined as

$$\varkappa = \frac{\sqrt{2mJ}}{\hbar}. \tag{17}$$

It is important to note that $J = 0.1$ eV and $\varkappa a = 3$ corresponds to the skyrmion size $d = 3.7$ nm, which is close to the experimentally found skyrmions in a PdFe bilayer on the Ir(111) surface.[30,31] In general, all spin-up and spin-down of σ_{xx} are the growing functions with ε_F. However, at small skyrmion sizes, $\varkappa a = 3$, the spin-up component (see the insertion at Fig. 4a) exhibits the small dip at the Fermi energy close to the bottom of the upper band ($\varepsilon_F \approx 2J$). At higher temperatures, the dip is smoothed out by the temperature smearing, while the dependence is more pronounced at lower temperatures (the red curve). As shown in Figs. 4d, e, f, the spin-down σ_{xx} vanishes below the threshold ($\varepsilon_F < 2J$), which is equal to $2JS_0$ at $T = 0$. Because of non-zero temperature, the levels in the upper curve become populated by electrons and, therefore, contribute to current. In Fig. 5 we present the temperature dependencies of σ_{xx} for the spin-up (Figs. 5a, b, and c) and spin-down projections (Figs. 5d, e, and f). The red curve represents ε_F close to the bottom of the lower band, i. e., the concentration of spin-up electrons is very low and, therefore, the value of the conductivity is close to zero. For the spin-down component it is always zero due to inequality (16). In general, the spin-down components of electric conductivity for different skyrmion sizes and Fermi energies close to the bottom of the upper energy band (the blue and green curves) are the growing functions with temperature. However, the spin-up components being slightly above the threshold (the green curves), behave differently at the small and medium skyrmion sizes and have the minimum at $k_BT \approx 0.1J$. The minimum can be explained from the analysis of Figs. 4a and b. Indeed, we see small dips at Fermi energy slightly below the threshold, which is exactly the case for Figs. 5a, b. For the larger skyrmion size $\varkappa a = 15$, the spin-up σ_{xx} is only the growing function.

B. Spin-dependent Hall current

In this subsection we present the results of the calculations of the spin-dependent Hall component of electric current. The spin-up component exists in the whole range of ε_F. We consider the three different skyrmion sizes: $\varkappa a = 3$, $\varkappa a = 5$, $\varkappa a = 15$. The most dramatic behavior is observed for the small and intermediate skyrmion sizes. At $\varkappa a = 3$, we find the σ_{xy} absolute value maximum close to the bottom of the upper band where the substantial temperature effects are observed. The higher the temperature, the smaller the Hall conductivity. The values of the σ_{xy} are negative, i. e., the Hall current is directed

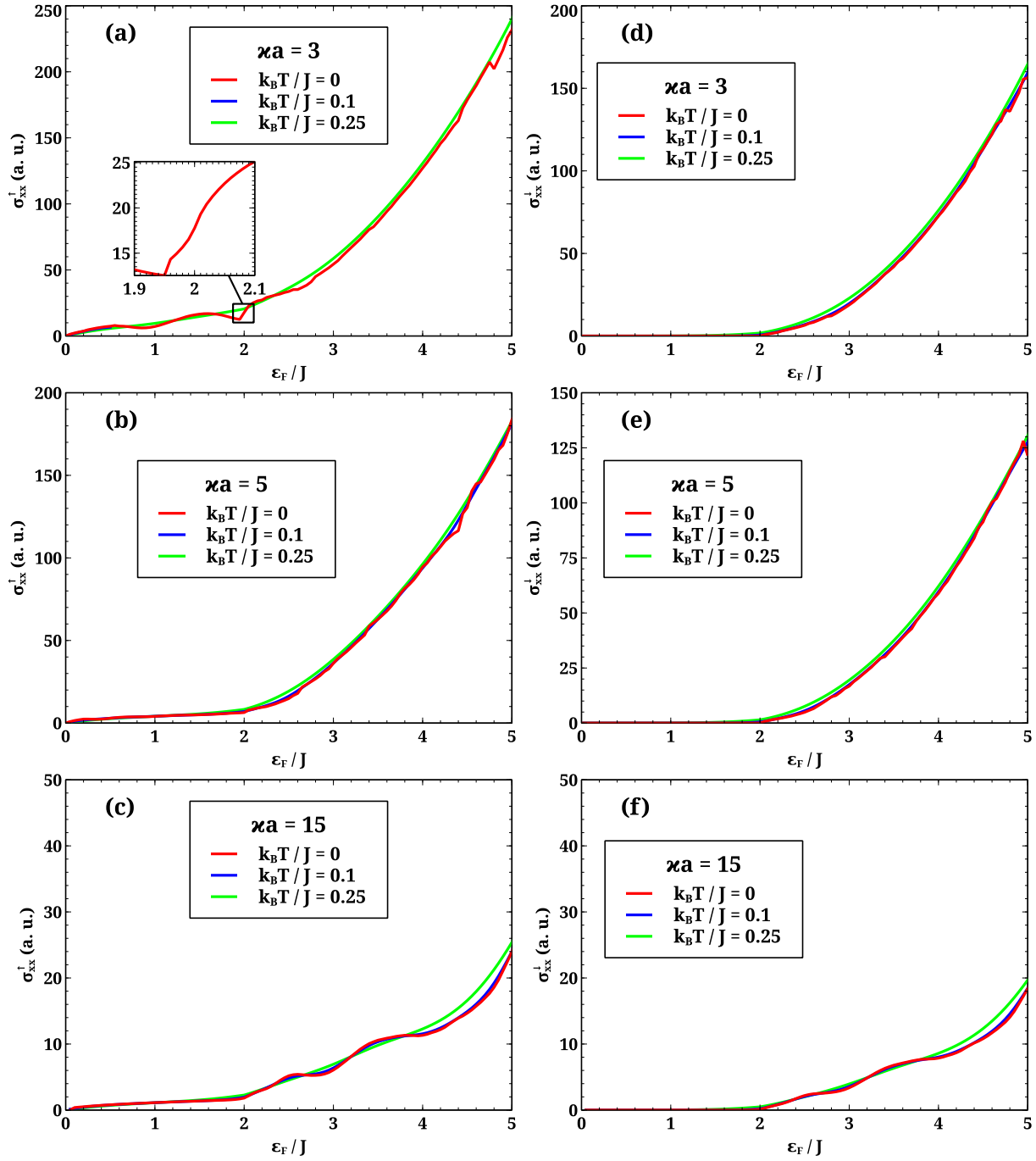

FIG. 4. Dependence of the direct conductivity, σ_{xx}, on Fermi energy. (a), (b), and (c) represent conductivity for spin-up electrons. (d), (e), and (f) represent conductivity for spin-down electrons. The skyrmion sizes are $\varkappa a = 3$, $\varkappa a = 5$, and $\varkappa a = 15$.

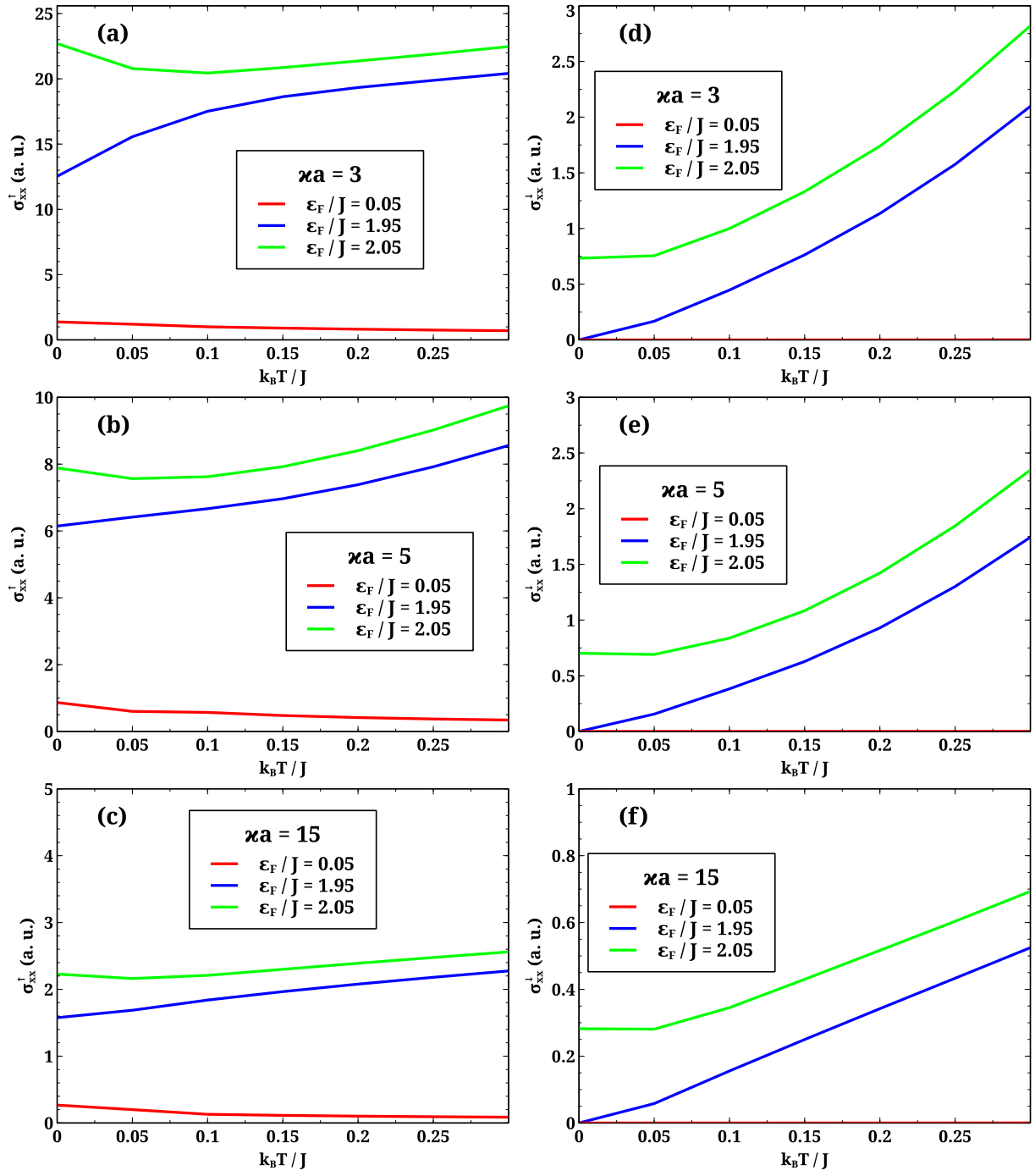

FIG. 5. Dependence of the direct conductivity, σ_{xx}, on temperature. (a), (b), and (c) represent conductivity for spin-up electrons. (d), (e), and (f) represent conductivity for spin-down electrons. The skyrmion sizes are $\varkappa a = 3$, $\varkappa a = 5$, and $\varkappa a = 15$.

to the right of the electric field. The minimum in the Hall conductivity absolute value (the maximum in Fig. 6a) is located at $\varepsilon_F = 3.4J$. We find a similar behavior for the skyrmion with the medium size ($\varkappa a = 5$), as shown in Fig. 6b. In this case, the maximum is at $\varepsilon_F = 3.8J$, and the minimum is located at $\varepsilon_F = 4.4J$. For the skyrmion of the large size, $\varkappa a = 15$, the absolute value the of spin-up Hall conductivity monotonically increases with Fermi energy. For this skyrmion size, the spin-up component of the Hall conductivity is negative as well. The absolute values of the spin-up Hall conductivity increase with skyrmion size.

The spin-down component of the Hall conductivity exhibits even more dramatic behavior than that of the spin-up conductivity. Indeed, there is the threshold value where for $\varepsilon_F < 2J$ the spin-down conductivity is zero (see Figs. 6d, e, and f). For the small skyrmion size, $\varkappa a = 3$, the Hall conductivity is negative while for $\varkappa a = 5$ and $\varkappa a = 15$, it is positive. In Fig. 6d the spin-down Hall conductivity demonstrates the small maximum only at $k_B T = 0$ in the vicinity of the threshold value, $\varepsilon_F = 2J$. After that, the sign of the Hall conductivity changes to negative values and reaches the absolute value maximum (the minimum in Fig. 6d) at $\varepsilon_F = 2.9J$. At the larger values of ε_F, we observe several smaller maxima and minima in the Hall conductivity. In the case of the medium skyrmion size, $\varkappa a = 5$, the value of σ_{xy} is always positive. At $\varepsilon_F = 3J$ there is the broad maximum, and the minimum at $\varepsilon_F = 3.6J$. The sharp maximum can be also found at $\varepsilon_F = 4.4J$. In the case of the large skyrmion size, $\varkappa a = 15$, the spin-down Hall conductivity monotonically increases from the threshold value of $\varepsilon_F = 2J$. We should mention that there is the nonvanishing values of the spin-down Hall conductivity for $\varepsilon_F < 2J$ at nonzero temperatures for all three skyrmion sizes.

As shown in Figs. 7a, b, and c, the spin-up Hall conductivity is negative for all skyrmion sizes. The most interesting effect occurs when the absolute value has the broad maximum for $\varepsilon_F = 1.95J$ (the minimum in Fig. 7a, the blue curve) at $k_B T = 0.075J$. From the general point of view, one would expect the increase of the conductivity amplitude with temperature. However, Fig. 7a demonstrates that initially the absolute value of the conductivity increases, reaches the maximum, and then drops. For the medium and larger skyrmion sizes, the absolute value of the conductivity monotonically decreases with the temperature.

The temperature dependences of the spin-down Hall conductivity are shown in Figs. 7d, e, and f. For the skyrmions with sizes $\varkappa a = 5$ and $\varkappa a = 15$, the conductivities are positive and monotonically grow with temperature from the threshold value for all ε_F values. We

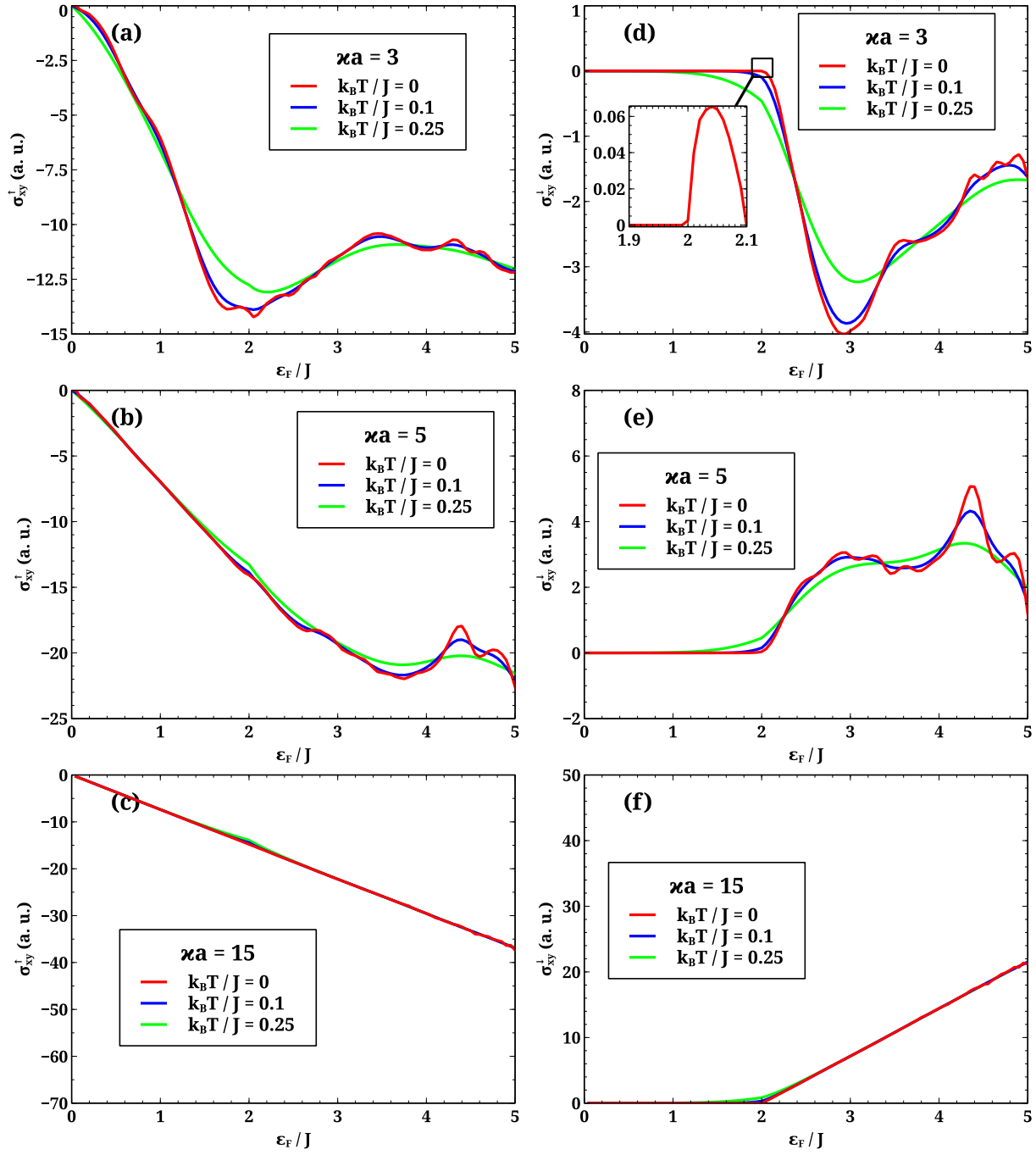

FIG. 6. Dependence of the Hall conductivity, σ_{xy}, on Fermi energy. (a), (b), and (c) represent conductivity for spin-up electrons. (d), (e), and (f) represent conductivity for spin-down electrons. The skyrmion sizes are $\varkappa a = 3$, $\varkappa a = 5$, and $\varkappa a = 15$.

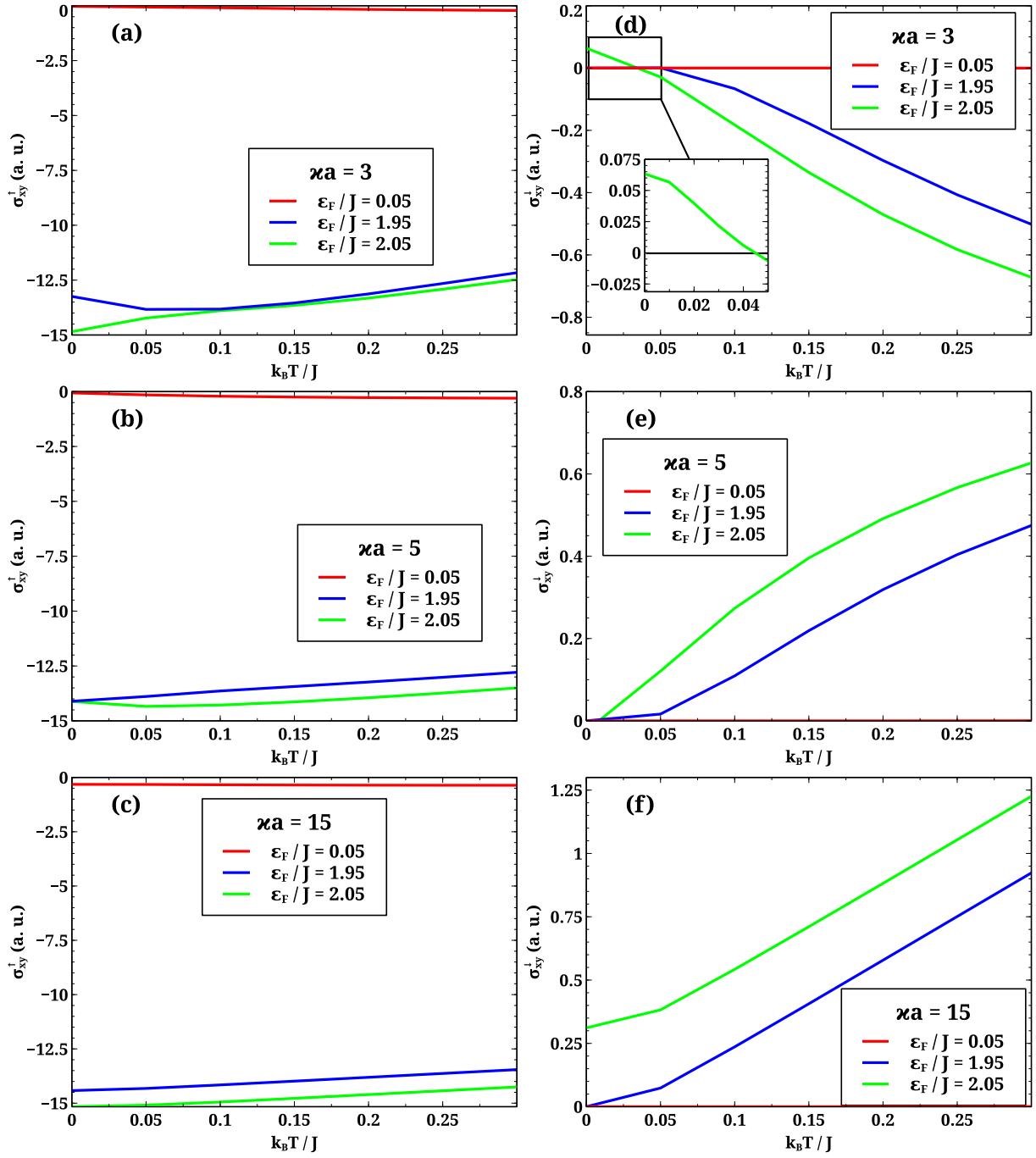

FIG. 7. Dependence of the Hall conductivity, σ_{xy}, on temperature. (a), (b), and (c) represent conductivity for spin-up electrons. (d), (e), and (f) represent conductivity for spin-down electrons. The skyrmion sizes are $\varkappa a = 3$, $\varkappa a = 5$, and $\varkappa a = 15$.

find the most interesting effects for the small skyrmion sizes, $\varkappa a = 3$, and $\varepsilon_F = 2.05J$ (the green curve): (a) the conductivity changes the sign in the vicinity of $k_BT = 0.04J$ (see the insertion in Fig. 7d) and (b) the absolute value initially decreases to zero at $k_BT = 0.04J$ and then monotonically increases. The largest absolute values of the Hall conductivity for both spin-up and spin-down Hall conductivity are observed for the Fermi energy above the threshold value, $2J$.

In order to reflect the existence of emergent magnetic fields in the case where the electron scatters by the spin texture we present the Hall resistivity in terms of the well-known formula:

$$\rho^s_{yx} = \frac{B^s_T}{eN^s c}, \tag{18}$$

where B^s_T is the effective topological "magnetic" field[13,27], N^s is the concentration of electrons with spin s, which is defined from the following expression:

$$N^s = \frac{1}{(2\pi)^2} \int \frac{\mathrm{d}^2\mathrm{k}}{\exp\left(\frac{\varepsilon_s(k)-\mu(\varepsilon_F,T)}{k_BT}\right)+1}, \tag{19}$$

and $\varepsilon_s(\boldsymbol{k})$ can be determined from expression (12). ρ^s_{yx} can be presented in terms of spin-dependent conductivities in the following way:

$$\rho^s_{yx} = \frac{\sigma^s_{yx}}{\left(\sigma^s_{xx}\right)^2 + \left(\sigma^s_{yx}\right)^2}. \tag{20}$$

We have numerically calculated the Fermi energy dependence of $B^{\uparrow}_T$ and $B^{\downarrow}_T$ as shown in Figs. 8 (a) and (b).

From Figs. 8 (a) and (b) we conclude that the sign of B_T depends on spin projection. It is remarkable that the effective topological "magnetic"field is negative for spin-up and positive for spin-down. The absolute value has the maxima and minima for both components. Indeed, the absolute value of $B^{\uparrow}_T$ (Fig. 8a) initially grows and then drops with some oscillations. $B^{\downarrow}_T$ is always positive and slightly drops with ε_F exhibiting soma maxima and minima. In ordinary Hall effect B is a constant, which is spin-independent. Thus, the effective topological "magnetic" field is very far from mapping onto an ordinary magnetic field. Moreover, the topological "magnetic" field depends on temperature. The discrepancy is large for small ε_F.

If we suggest that the Hall effect consists of the two contributions: (a) the anomalous Hall effect and (b) the topological Hall effect, then the only contribution is due to the anomalous

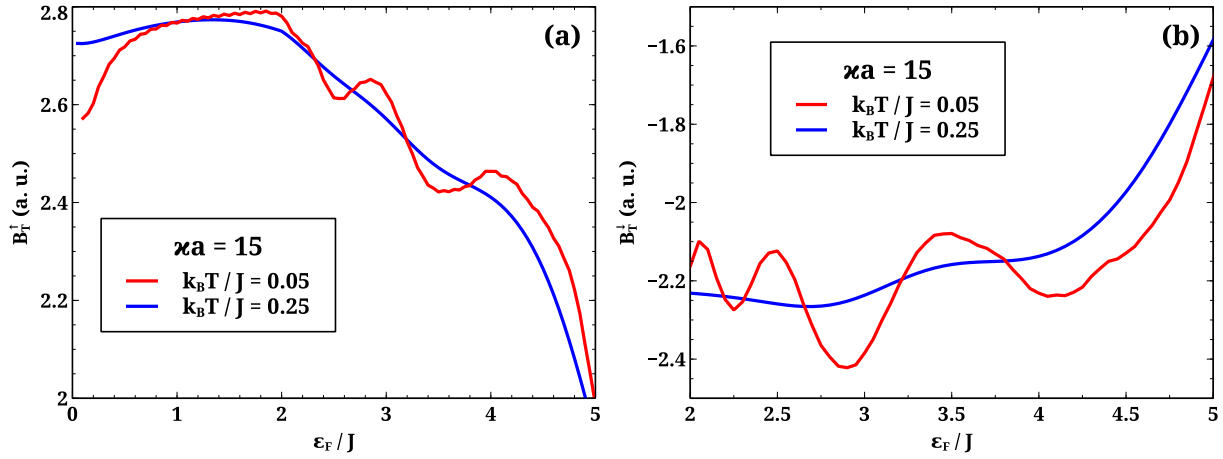

FIG. 8. Effective topological "magnetic" field (a) $B_T^{\uparrow}$ and (b) $B_T^{\downarrow}$ depending on ε_F for two different temperatures: the red line for $k_BT = 0.05J$ and the blue line $k_BT = 0.25J$. The skyrmion size is chosen $\varkappa a = 15$.

Hall effect in the absence of skyrmions. In this case it is necessary to introduce additional scattering mechanisms that are not in the scope of this work. However, we study the direct and Hall resistances with respect to JS_0 representing the ferromagnetic moment. The dependencies of the resistivity ρ on J for different spins and projections at zero temperature are presented in Figs. 9.

As shown in Figs. 9 (a) and (c), the spin-up resistivity becomes the constant after some threshold value of $2J = \varepsilon_F$. The threshold value implies that the second energy band (see Fig. 1) that is in charge of the spin-down electron scattering, is empty. For $2J > \varepsilon_F$ the spin-down component of the resistivity is the constant independent of J. This property can be explained by adiabatic regime of scattering and emptiness of the upper band. As far as the spin-down components are concerned, the resistivities are the growing functions with J when $2J < \varepsilon_F$. For $2J > \varepsilon_F$ the spin-down resistivity is ∞. As we have discussed above the separation of the anomalous and topological spin Hall effects are impossible.

IV. CONCLUSIONS

In this work we have studied a system of both localized and delocalized electrons where the localized electrons provide the magnetic moments described by skyrmions in a ferromagnetic environment (see Eq. (2)). The skyrmions are considered to be static and are not influenced

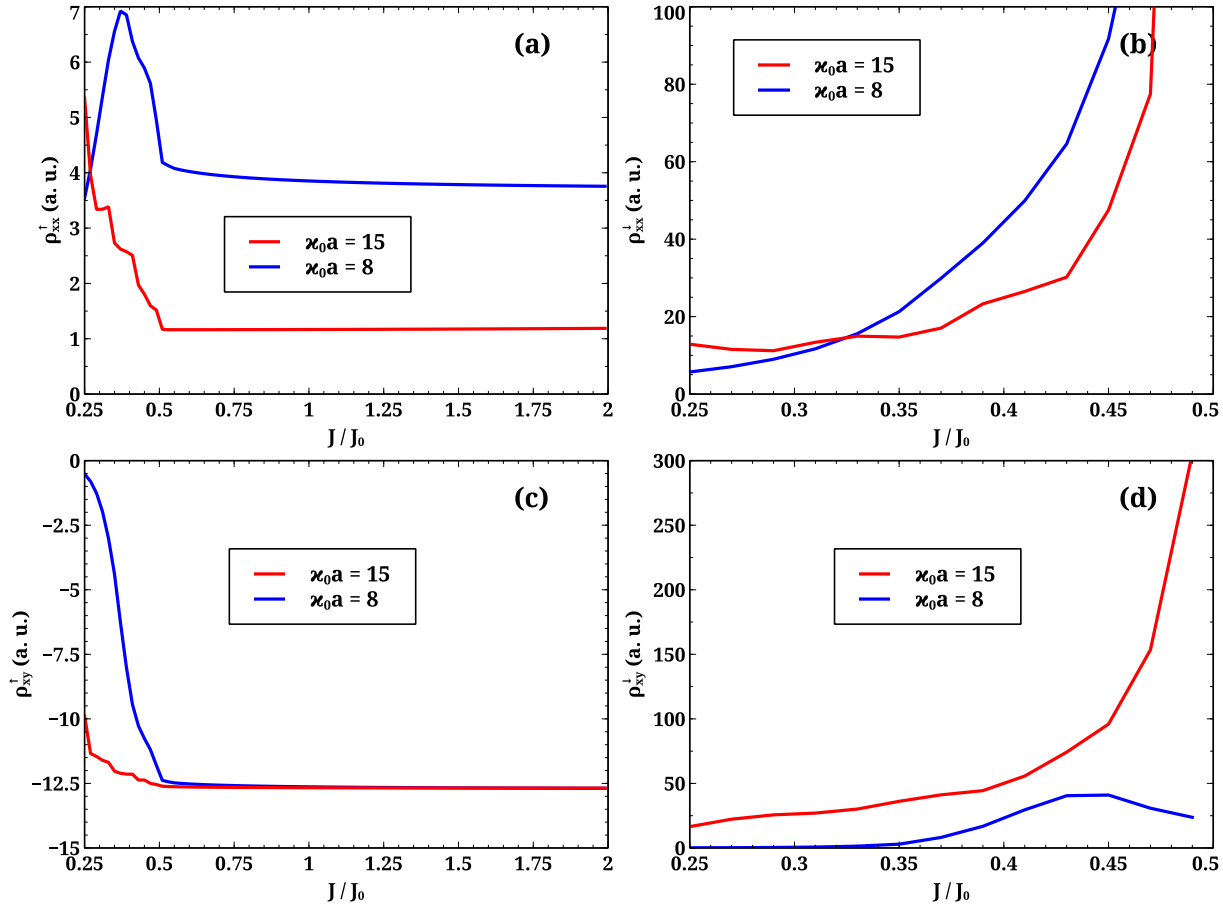

FIG. 9. Dependencies of the resistivity on the ferromagnetic moment J: (a) direct resistivity $\rho^{\uparrow}_{xx}$, (b) direct resistivity $\rho^{\downarrow}_{xx}$, (c) Hall resistivity $\rho^{\uparrow}_{xy}$, and (d) Hall resistivity $\rho^{\downarrow}_{xy}$ for the skyrmion size $\varkappa a = 15$ and $\varepsilon_F = 0.1$ eV.

by electric current and temperature. The 2D free electron gas scatters by the magnetic textures providing spin-dependent Hall currents. When skyrmion sizes are very small or skyrmions vanish, the electron scattering mechanism by skyrmions becomes invalid because of the lack of scatters. In this case other scattering mechanisms such as electron-phonon interaction, magnetic and nonmagnetic impurities have to be introduced into the Boltzmann equation. In this work we consider only the electron-skyrmion scattering mechanism. The band structure of 2D electrons is shown in Fig. 1. For the direct spin-up conductivities (see Fig. 5a) we find the nonmonotonic behavior of the conductivity with temperature. Indeed, the absolute value initially decreases to the minimum at $k_BT = 0.1J$, and then increases at higher temperatures. Due to the scattering of the free electrons by the skyrmions, we have

found substantial nonlinear behaviors in the spin-up and spin-down Hall conductivities. In general, one would expect the monotonic increase of conductivity with temperature. However, as shown in Fig. 7a, the absolute value of the Hall conductivity initially increases and then decreases with temperature. Such a behavior is unusual. Moreover, as shown in Fig. 7d, the spin-down Hall conductivity changes the sign from positive to negative at $k_BT = 0.04J$ exhibiting the minimum in the absolute value of the conductivity at this point. A skyrmion size is essential because this effect does not exist for larger skyrmion sizes. In this work we have chosen the skyrmion sizes of $\varkappa a = 3, 5$, and 15 corresponding to $d = 3.7,\ 6.2$, and 18.5 nm, respectively. Small skyrmions with $d = 3.7$ nm were experimentally observed in a PdFe bilayer on the Ir(111) surface.[30,31] If we present the Hall resistivity in terms of the well-known formula for the Hall resistivity (see Eq. (18)), we find the interesting dependencies of the B_T-components with respect of ε_F as shown in Figs. 8. The absolute values of the spin-up and spin-down B_T-components decrease with ε_F. B_T for spin-up and spin-down conductivities have different signs. The same sing difference in the emergent magnetic field approach due to the presence of skyrmions[27] was also found. As shown in Figs. 9, the spin-up components of the resistivity are independent of the exchange integral J when $2J > \varepsilon_F$. However the spin-down resistivities are the growing functions when $2J < \varepsilon_F$. For $2J > \varepsilon_F$ the spin-down resistivity is infinite. The found effects can be useful for the applications in logic memory elements based on skyrmions in classical and quantum computing.

ACKNOWLEDGMENTS

This work was supported by a grant from the U S National Science Foundation (No. DMR-1710512) and the U S Department of Energy (No. 1004389) to the University of Wyoming.

APPENDIX

HELICITY INDEPENDENCE

In this section the independence of scattering properties of a skyrmion (or for any magnetic texture) helicity is proved for the most general case. We present the magnetic moment

distribution in the following way:

$$S_z = S_z(\boldsymbol{r}), \quad S_x = S_{\parallel}(\boldsymbol{r}) \cos(\varphi(\boldsymbol{r}) + \varphi_0), \quad S_y = S_{\parallel}(\boldsymbol{r}) \sin(\varphi(\boldsymbol{r}) + \varphi_0). \tag{A-I.1}$$

The perturbation operator $\hat{V}$ in this case is taken as follows:

$$\hat{V} = -J \begin{pmatrix} S_z(\boldsymbol{r}) & e^{-i\varphi_0} S^-(\boldsymbol{r}) \\ e^{i\varphi_0} S^+(\boldsymbol{r}) & -S_z(\boldsymbol{r}) \end{pmatrix}, \tag{A-I.2}$$

where $S^{\pm}(\boldsymbol{r}) = S_{\parallel}(\boldsymbol{r}) e^{\pm i\varphi(\boldsymbol{r})}$ are functions independent of φ_0. For further convenience it can be rewritten as follows:

$$\hat{V} = V_{ss'}(\boldsymbol{r}) e^{i\nu_{ss'}\varphi_0}, \tag{A-I.3}$$

where $\nu_{\uparrow\uparrow} = \nu_{\downarrow\downarrow} = 0$, $\nu_{\uparrow\downarrow} = -1$. and $\nu_{\downarrow\uparrow} = 1$.

It can be explicitly proven that for any $s_1 = \uparrow, \downarrow$

$$\nu_{ss_1} + \nu_{s_1 s'} = \nu_{ss'}$$

If we rewrite the $\hat{V}$-operator in the k-space, the result is transformed in the following way:

$$\left\langle \boldsymbol{k}s \middle| \hat{V} \middle| \boldsymbol{k}'s' \right\rangle = V_{ss'}(\boldsymbol{k}, \boldsymbol{k}') e^{i\nu_{ss'}\varphi_0}, \tag{A-I.4}$$

where $V_{ss'}(\boldsymbol{k}, \boldsymbol{k}')$ is independent of φ_0. Substituting this expression into Lippmann-Schwinnger equation (7), we can write this equation in the integral form:

$$\begin{aligned} &\left\langle \boldsymbol{k}s \middle| \hat{T} \middle| \boldsymbol{k}'s' \right\rangle = V_{ss'}(\boldsymbol{k}, \boldsymbol{k}') e^{i\nu_{ss'}\varphi_0} + \\ &\sum_{s_1} e^{i\nu_{ss_1}\varphi_0} \int V_{ss'}(\boldsymbol{k}, \boldsymbol{k}') G_0^{s_1}(\boldsymbol{k}_1) \left\langle \boldsymbol{k}_1 s_1 \middle| \hat{T} \middle| \boldsymbol{k}'s' \right\rangle \mathrm{d^n k_1}, \end{aligned} \tag{A-I.5}$$

where n denotes a dimension ($n = 2$ stands for 2D and $n = 3$ for 3D materials). Using the form of $\left\langle \boldsymbol{k}s \middle| \hat{T} \middle| \boldsymbol{k}'s' \right\rangle = T_{ss'}(\boldsymbol{k}, \boldsymbol{k}') e^{i\nu_{ss'}\varphi_0}$, we obtain the following equation (here $T_{ss'}(\boldsymbol{k}, \boldsymbol{k}')$ is independent of φ_0):

$$\begin{aligned} &T_{ss'}(\boldsymbol{k}, \boldsymbol{k}') e^{i\nu_{ss'}\varphi_0} = V_{ss'}(\boldsymbol{k}, \boldsymbol{k}') e^{i\nu_{ss'}\varphi_0} + \\ &\sum_{s_1} e^{i\left(\nu_{ss_1} + \nu_{s_1 s'}\right)\varphi_0} \int V_{ss'}(\boldsymbol{k}, \boldsymbol{k}') G_0^{s_1}(\boldsymbol{k}_1) T_{ss'}(\boldsymbol{k}, \boldsymbol{k}') \mathrm{d^n k_1} = \\ &V_{ss'}(\boldsymbol{k}, \boldsymbol{k}') e^{i\nu_{ss'}\varphi_0} + e^{i\nu_{ss'}\varphi_0} \sum_{s_1} \int V_{ss'}(\boldsymbol{k}, \boldsymbol{k}') G_0^{s_1}(\boldsymbol{k}_1) T_{ss'}(\boldsymbol{k}, \boldsymbol{k}') \mathrm{d^n k_1}. \end{aligned} \tag{A-I.6}$$

Thus, the final form of the Lippman-Schwinger equation becomes independent of φ_0:

$$T_{ss'}\left(\boldsymbol{k},\boldsymbol{k}'\right)=V_{ss'}\left(\boldsymbol{k},\boldsymbol{k}'\right)+\sum_{s_1}\int V_{ss'}\left(\boldsymbol{k},\boldsymbol{k}'\right)G_0^{s_1}\left(\boldsymbol{k}_1\right)T_{ss'}\left(\boldsymbol{k},\boldsymbol{k}'\right)\mathrm{d^n k_1}. \tag{A-I.7}$$

In order to substitute T-matrix into the Boltzmann equation we have to square its absolute value:

$$W_{\boldsymbol{k}\boldsymbol{k}'}^{ss'}=\frac{2\pi}{\hbar}n_t\left|\left\langle \boldsymbol{k}s\right|\hat{T}\left|\boldsymbol{k}'s'\right\rangle\right|^2\delta(\varepsilon-\varepsilon'), \tag{A-I.8}$$

where $|e^{i\nu_{ss'}\varphi_0}|=1$. Thus, we have proved that the scattering properties are independent of the helicity φ_0. In particular, Neel, $\varphi_0=0$, and Bloch, $\varphi_0=\pi/2$, skyrmions would identically scatter electrons. For the proof it is important to use the representation where the wave functions are the eigenfunctions of the Hamiltonian $\hat{H}_0$. The derivations presented above are valid for any spin texture including skyrmions and any energy band shape.

---

* yurid@uwyo.edu

[1] N. Nagaosa and Y. Tokura, Nat. Nanotechnol. **8**, 899–911 (2013).

[2] A. Fert, V. Cros, and J. Sampaio, Nat. Nanotechnol. **8**, 152–156 (2013).

[3] W. Jiang, G. Chen, K. Liu, J. Zang, S. Velthuis, and A. Hoffmann, Phys. Rep. **704** (2017).

[4] S. Li, W. Kang, X. Zhang, T. Nie, Y. Zhou, K. Wang, and W. Zhao, Mater. Horizons (2020).

[5] G. Yang, P. Stano, J. Klinovaja, and D. Loss, Phys. Rev. B **93** (2016).

[6] E. Mascot, J. Bedow, M. Graham, S. Rachel, and D. K. Morr, npj Quantum Mater. **6**, 6 (2021).

[7] K. von Bergmann, A. Kubetzka, O. Pietzsch, and R. Wiesendanger, J. Phys. Condens. Matter. **26**, 394002 (2014).

[8] J. Iwasaki, M. Mochizuki, and N. Nagaosa, Nat. Commun. **4**, 1463 (2013).

[9] T. Schulz, R. Ritz, A. Bauer, M. Halder, M. Wagner, C. Franz, C. Pfleiderer, K. Everschor, M. Garst, and A. Rosch, Nat. Phys. **8**, 301–304 (2012).

[10] F. Jonietz, S. Mühlbauer, C. Pfleiderer, A. Neubauer, W. Münzer, A. Bauer, T. Adams, R. Georgii, P. Böni, R. A. Duine, et al., Science **330**, 1648 (2010).

[11] X. Yu, N. Kanazawa, W. Zhang, T. Nagai, T. Hara, K. Kimoto, Y. Matsui, Y. Onose, and Y. Tokura, Nat. Commun. **3**, 988 (2012).

[12] K. S. Denisov, I. V. Rozhansky, N. S. Averkiev, and E. Lähderanta, Phys. Rev. Lett. **117**, 027202 (2016).

[13] K. S. Denisov, I. V. Rozhansky, N. S. Averkiev, and E. Lähderanta, Phys. Rev. B **98**, 195439 (2018).

[14] N. A. Sinitsyn, J. Phys. Condens. Matter **20**, 023201 (2007).

[15] A. Zadorozhnyi and Y. Dahnovsky, J. Phys. Condens. Matter **32**, 405803 (2020).

[16] C. Fang, C. Wan, C. Guo, C. Feng, X. Wang, Y. Xing, M. Zhao, J. Dong, G. Yu, Y. Zhao, et al., Appl. Phys. Lett. **115**, 212402 (2019).

[17] J. Xu, W. A. Phelan, and C.-L. Chien, Nano Lett. **19**, 8250 (2019).

[18] C. D. W. Cox, A. J. Caruana, M. D. Cropper, and K. Morrison, J. Phys. D. **53**, 035005 (2019).

[19] P. Sheng, Y. Sakuraba, Y. Lau, S. Takahashi, S. Mitani, and M. Hayashi, Sci. Adv. **3**, 1701503 (2017).

[20] A. S. Melo, A. B. d. Oliveira, C. Chesman, R. D. Della Pace, F. Bohn, and M. A. Correa, Sci. Rep. **9**, 15338 (2019).

[21] M. Mizuguchi and S. Nakatsuji, Sci Technol Adv Mater **20**, 262 (2019).

[22] R. Ramos, M. Aguirre, A. Anadón, J. Blasco, I. Lucas, P. Algarabel, L. Morellón, E. Saitoh, and M. Ibarra, Phys. Rev. B **90**, 054422 (2014).

[23] K. Uchida, S. Takahashi, K. Harii, J. Ieda, W. Koshibae, K. Ando, S. Maekawa, and E. Saitoh, Nature **455**, 778 (2008).

[24] A. Anselm, *Introduction to Semiconductor Theory* (Mir, Moscow, 1981).

[25] A. Zadorozhnyi and Y. Dahnovsky, J. Magn. Magn. Mater **518**, 167367 (2021).

[26] S. S. Pershoguba, S. Nakosai, and A. V. Balatsky, Phys. Rev. B **94**, 064513 (2016).

[27] Y. Tokura and N. Nagaosa, Phys. Scr. **2012**, 014020 (2012).

[28] J. R. Taylor, *Scattering Theory: The quantum Theory on Nonrelativistic Collisions* (Wiley, New York, 1972).

[29] L. Landau and E. Lifshitz, *Statistical Physics: Volume 5* (Elsevier Science, 2013).

[30] X. S. Wang, H. Y. Yuan, and X. R. Wang, Commun. Phys. **1**, 31 (2018).

[31] N. Romming, C. Hanneken, M. Menzel, J. E. Bickel, B. Wolter, K. von Bergmann, A. Kubetzka, and R. Wiesendanger, Science **341**, 636 (2013).